
Fast-DDPM: Fast Denoising Diffusion Probabilistic Models for Medical Image-to-Image Generation

Hongxu Jiang¹ Muhammad Imran¹ Linhai Ma¹ Teng Zhang¹
Yuyin Zhou² Muxuan Liang¹ Kuang Gong¹ Wei Shao^{1*}

¹University of Florida, FL, USA ²University of California, Santa Cruz, CA, USA
{hongxu.jiang, muhammad.imran, l.ma, zhangt, muxuan.liang, weishao}@ufl.edu
yzhou284@ucsc.edu kgong@bme.ufl.edu

Abstract

Denoising diffusion probabilistic models (DDPMs) have achieved unprecedented success in computer vision. However, they remain underutilized in medical imaging, a field crucial for disease diagnosis and treatment planning. This is primarily due to the high computational cost associated with (1) the use of large number of time steps (e.g., 1,000) in diffusion processes and (2) the increased dimensionality of medical images, which are often 3D or 4D. Training a diffusion model on medical images typically takes days to weeks, while sampling each image volume takes minutes to hours. To address this challenge, we introduce Fast-DDPM, a simple yet effective approach capable of improving training speed, sampling speed, and generation quality simultaneously. Unlike DDPM, which trains the image denoiser across 1,000 time steps, Fast-DDPM trains and samples using only 10 time steps. The key to our method lies in aligning the training and sampling procedures to optimize time-step utilization. Specifically, we introduced two efficient noise schedulers with 10 time steps: one with uniform time step sampling and another with non-uniform sampling. We evaluated Fast-DDPM across three medical image-to-image generation tasks: multi-image super-resolution, image denoising, and image-to-image translation. Fast-DDPM outperformed DDPM and current state-of-the-art methods based on convolutional networks and generative adversarial networks in all tasks. Additionally, Fast-DDPM reduced the training time to $0.2\times$ and the sampling time to $0.01\times$ compared to DDPM. Our code is publicly available at: <https://github.com/mirthAI/Fast-DDPM>.

1 Introduction

Diffusion models [9, 18, 31, 32] have become powerful tools for high-quality image generation [5]. The forward diffusion process incrementally adds noise to a high-quality image until it becomes pure Gaussian noise. An image denoiser is then trained to learn the reverse process, progressively removing noise from random Gaussian noise until it reconstructs a noise-free image. This enables the generation of new high-quality images that match the distribution of the training dataset. Beyond computer vision, diffusion models are increasingly applied to medical imaging [11, 15, 20, 29, 35] for improved disease diagnosis, treatment planning, and patient monitoring.

Training and sampling diffusion models are computationally expensive and time-consuming, especially for medical images. This is due to (1) the large number of discrete time steps needed to approximate the continuous diffusion process, (2) the need for large training datasets to model

*Corresponding author: Wei Shao, weishao@ufl.edu.

complex image distributions, and (3) the increased dimensionality of medical images from 2D to 3D and 4D. For 2D images, training can take days on a single GPU, while sampling can take several minutes per image [31]. These times scale significantly with 3D and 4D medical imaging volumes, posing challenges to practical usability. This extensive training time limits experimentation with different model architectures and hyperparameters, while the sampling time of minutes to hours per image volume limits the real-time clinical applications and the hospital throughput.

Current research mainly focuses on accelerating the sampling process, using either training-free or training-based methods [41]. Training-free methods utilize efficient numerical solvers for stochastic or ordinary differential equations to reduce the number of time steps required for sampling. This approach can decrease the number of sampling time steps from 1,000 to 50-100, without compromising the quality of the generated images. Alternatively, training-based methods, such as progressive knowledge distillation [26, 30], can further reduce the sampling steps to as few as 10. However, this approach requires the training of additional student models, which considerably increases the overall training cost and may not be practical for medical image analysis.

In this paper, we propose Fast-DDPM, a model designed to reduce both training and sampling times by optimizing time-step utilization. We observed that the majority of time steps involved in training are not utilized by faster diffusion samplers during sampling. For instance, a Denoising Diffusion Probabilistic Model (DDPM) trained with 1,000 time steps is often sampled by the Denoising Diffusion Implicit Model (DDIM) using only 100 time steps. This practice is resource-inefficient, as the image denoiser is trained on 900 time points that are ultimately skipped during sampling. To address this inefficiency in training, we propose training and sampling the DDPM model at the same 10 time steps, as illustrated in Figure 1. We evaluated Fast-DDPM on three medical image-to-image

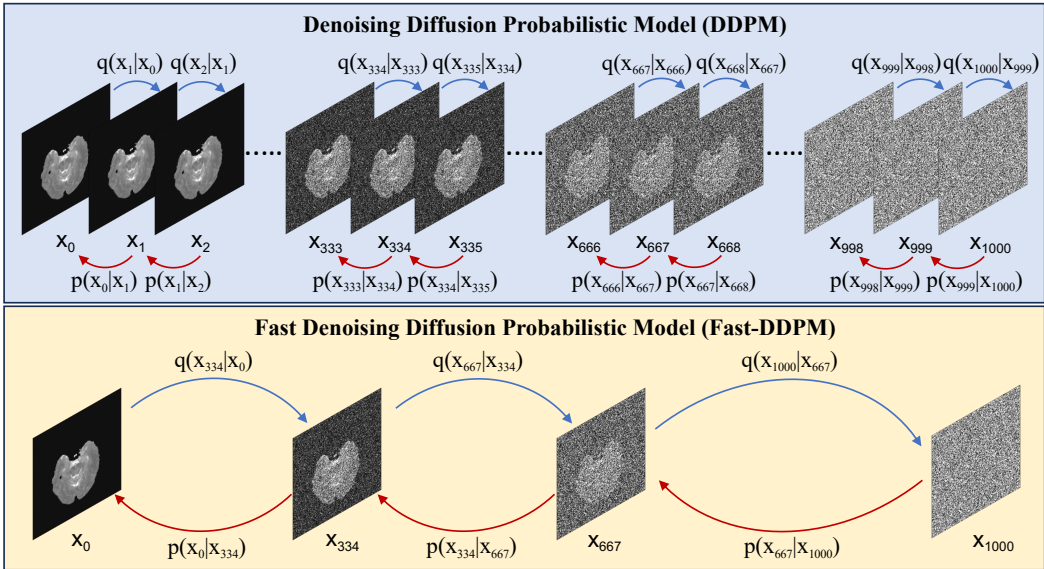


Figure 1: Fast-DDPM uses significantly fewer time steps than DDPM. For illustration purposes, we used only 3 time steps for Fast-DDPM in this example.

tasks, including multi-image super-resolution for prostate MRI, denoising low-dose CT scans, and image-to-image translation for brain MRI. Fast-DDPM achieved state-of-the-art performance across all three tasks. Notably, Fast-DDPM is approximately 100 times faster than the DDPM model during sampling and about 5 times faster during training.

2 Related Work

Fast Sampling of Diffusion Models. Current methods to accelerate sampling of diffusion models can be classified as training-free and training-based. Training-free methods focus on developing diffusion solvers to efficiently solve reverse stochastic differential equations or their equivalent ordinary differential equations (ODEs). For instance, the DDIM sampler [31] models the reverse diffusion

process using an ODE, significantly reducing the sampling time steps to 100 without impacting generation quality. DPM-Solver [22] introduces a high-order solver for diffusion ODEs based on an exact solution formulation that simplifies to an exponentially weighted integral, achieving high-quality sample generation with just 10-50 steps. A common training-based approach is knowledge distillation, where a teacher diffusion model is initially trained with a large number of time steps, followed by the sequential training of multiple student models with progressively fewer time steps, mirroring the teacher model’s behavior [26, 30]. This method reduces sampling time steps from 1,000 to 16 while maintaining sampling quality.

Diffusion Models in Medical Imaging. Diffusion models have been applied to various medical imaging tasks, including segmentation [11, 16, 39], anomaly detection [13, 37, 40], denoising [4, 7, 24], reconstruction [1, 8, 21], registration [15], super-resolution [4, 24, 35, 38], and image-to-image translation [17, 23, 29]. Among these, the DDPM model is the most widely used in medical imaging due to its simplicity. Diffusion models can be categorized as 2D, 3D, or 4D based on input image dimensions. Currently, 2D models are the predominant choice in medical imaging due to their ease of implementation and lower memory requirements. However, when implementing diffusion models for 3D and 4D applications, training can take significantly longer, lasting anywhere from weeks to months. Improving the training and sampling processes is crucial for a broader adoption of diffusion models in medical imaging.

3 Methods

3.1 Background

Diffusion Models. Starting from a noise-free image x_0 , the forward diffusion process is a continuously-time stochastic process from time $t = 0$ to $t = 1$, incrementally introducing noise to the image x_0 until it becomes pure Gaussian noise at $t = 1$. The distributions of the intermediate noisy images $x(t)$ are given by [18]:

$$q(x(t)|x_0) = \mathcal{N}(\alpha(t)x_0, \sigma^2(t)\mathbb{I}) \quad (1)$$

where $x(0) = x_0$, $\alpha(t)$ and $\sigma(t)$ are differentiable functions, and the signal-to-noise ratio function $\text{SNR}(t) := \frac{\alpha^2(t)}{\sigma^2(t)}$ decreases monotonically from $+\infty$ at $t = 0$ to 0 at $t = 1$. An equivalent formulation of $x(t)$ is given by the following stochastic differential equation (SDE):

$$dx(t) = f(t)x(t)dt + g(t)dW(t) \quad (2)$$

where $f(t) = \frac{\alpha'(t)}{\alpha(t)}$, $g(t) = \sqrt{(\sigma^2(t))' - 2\frac{\alpha'(t)}{\alpha(t)}\sigma^2(t)}$, and $W(t)$ is a standard Wiener process from $t = 0$ to $t = 1$. It has been shown that the reverse process of $x(t)$ is given by the following reverse-time SDE [32]:

$$dx(t) = [f(t) - g^2(t)\nabla_{x(t)} \log p(x(t))]dt + g(t)d\bar{W}(t) \quad (3)$$

where $x(1) = \mathcal{N}(0, \mathbb{I})$, $d\bar{W}(t)$ the standard Wiener process backwards from $t = 1$ to $t = 0$, and $p(x(t))$ denote the probability density of $x(t)$. If the score function $\nabla_{x(t)} \log p(x(t))$ is known for every $t \in [0, 1]$, one can solve the reverse-time SDE to sample new images.

We can train a model $s_\theta(x(t), t)$ to estimate the score function using the following loss function:

$$\mathbb{E}_{t \in [0, 1], x_0 \sim p_{\text{data}}, x(t) \sim q(x(t)|x_0)} \lambda(t) \|s_\theta(x(t), t) - \nabla_{x(t)} \log p(x(t)|x_0)\|_2^2 \quad (4)$$

where $p(x(t)|x_0)$ denote the density function of $x(t)$ generated in Eq. 1 and $\lambda(t)$ is a scalar-valued weight function. The training of $s_\theta(x(t), t)$ is straightforward since $q(x(t)|x_0)$ is a Gaussian distribution and its score function has a closed form:

$$\nabla_{x(t)} \log p(x(t)|x_0) = -\frac{x(t) - \alpha(t)x_0}{\sigma^2(t)} = -\frac{\epsilon}{\sigma(t)} \quad (5)$$

where ϵ is a random noise sample from $\mathcal{N}(0, \mathbb{I})$ to generate $x(t)$ from x_0 . Equivalently, we can use a U-Net denoiser $\epsilon_\theta(x(t), t)$ to estimate the random noise ϵ (i.e., the score function scaled by $-\sigma(t)$). Following [9], in this paper, we trained the U-Net denoiser using a simple loss function:

$$\mathbb{E}_{i \in [1, \dots, T], x_0 \sim p_{\text{data}}, \epsilon \sim \mathcal{N}(0, \mathbb{I})} [\epsilon - \epsilon_\theta(\alpha(t)x_0 + \sigma(t)\epsilon, t)]^2 \quad (6)$$

where T is the total number of time steps and $t = \frac{i}{T}$.

Linear- β Noise Scheduler. Any noise scheduler, defined by $\alpha(t)$ and $\sigma(t)$, should ensure that $\text{SNR}(1) = \frac{\alpha^2(1)}{\sigma^2(1)} \approx 0$ so that $x(1)$ is pure Gaussian noise. The variance-preserving noise schedulers [18] meet this requirement, where $\alpha(t)$ is a monotonically decreasing function, $\alpha(0) = 1$, $\alpha(1) = 0$, and $\alpha^2(t) + \sigma^2(t) = 1$ for all t . This formulation guarantees that the variance of any latent image $x(t)$ is bounded. The most popular variance-persevering noise scheduler is the linear- β noise scheduler used in the DDPM model [9]. In this approach, the forward diffusion process was defined as a Markovian process at discrete time steps $i \in \{1, 2, \dots, T\}$ using the following transition kernel:

$$q\left(x\left(\frac{i}{T}\right)\middle|x\left(\frac{i-1}{T}\right)\right) = \mathcal{N}\left(\sqrt{1 - \beta\left(\frac{i}{T}\right)}x\left(\frac{i-1}{T}\right), \beta\left(\frac{i}{T}\right)\mathbb{I}\right) \quad (7)$$

where $t = \frac{i}{T}$, $\beta(t) = 0.0001 + (0.02 - 0.0001)t$, and the corresponding α noise scheduler $\alpha(t)$ at discrete time steps is given by

$$\alpha\left(\frac{i}{T}\right) = \prod_{j=1}^i \left(1 - \beta\left(\frac{j}{T}\right)\right) \quad (8)$$

To establish feasible noise schedulers using Eq. 8, the total number of time steps T should be carefully chosen. Figure 2 plots $\alpha^2(t)$ for different choices of T : 100, 500, 1000, 2000, and 10000. As we can see, the total number of time steps cannot be too small (e.g., $T = 100$), as this results in the endpoint of the forward diffusion process $x(1)$ not being purely Gaussian. Conversely, if the total number of time steps is too large (e.g., $T = 10000$), $x(t)$ becomes pure Gaussian noise at an early time point (e.g., $t = 0.2$). This makes the training of $\epsilon_\theta(x(t), t)$ at time steps $t > 0.2$ unnecessary since there is no change in the noise level of $x(t)$ beyond this point. The plots in Figure 2 suggest that a good choice of T lies between 500 and 2000. This explains why a linear- β noise scheduler with $T = 1000$ is currently the most popular choice [9]. In other words, we cannot reduce the number of time steps to 10 using Eq. 8. In this study, we first define the continuous function $\alpha^2(t)$ and then sample it at discrete time points.

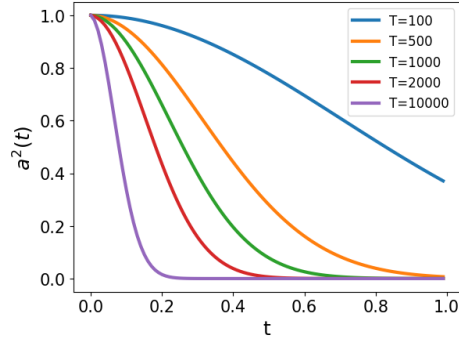


Figure 2: Impact of the number of time steps, T , on the noise scheduler.

3.2 Fast Denoising Diffusion Probabilistic Model (Fast-DDPM)

We have developed the Fast-DDPM model to accelerate the training and sampling of DDPM by utilizing task-specific noise schedulers with only 5-10 time steps.

Task-Specific α Noise Scheduler. Previous studies indicate that images of different sizes require different noise schedulers for optimal results [3, 10]. Inspired by this, we propose two α noise schedulers for various medical image-to-image tasks. We first define a smooth, monotonically decreasing function $\alpha^2(t)$ from $t = 0$ to $t = 1$, with boundary conditions $\alpha^2(0) = 1$ and $\alpha^2(1) = 0$. In this paper, we use $\alpha^2(t)$ as defined by the linear- β noise scheduler with $T = 1,000$ in Eq.8 (see the green curve in Figure 2). Unlike the linear- β noise scheduler used in the DDPM model, which uniformly samples 1,000 time points between $[0,1]$, our first proposed noise scheduler uniformly samples 10 time steps between $[0,1]$ (Figure 3(a)). The second proposed noise scheduler non-uniformly samples 10 time points between $[0,1]$, with denser sampling at higher noise levels (Figure 3(b)). This formulation of noise schedulers satisfies all the desirable properties outlined earlier. Due to the reduced training and sampling time, users have the opportunity to try both noise schedulers for each image-to-image task to determine which one fits their task better.

We provide a rationale for our design. Previous works [31, 32] have demonstrated that the sampling process is equivalent to solving a reverse-time ODE of the image flow starting from $x(1) \sim \mathcal{N}(0, \mathbb{I})$. In a related context of diffeomorphic image registration, 10 time points are sufficient to solve an ODE

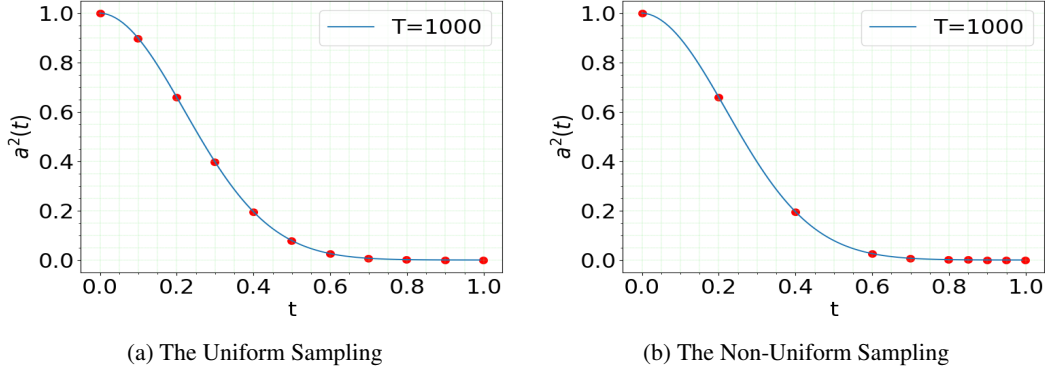


Figure 3: Proposed α noise schedulers with uniform and non-uniform sampling between $[0,1]$.

for accurately estimating a complex time-dependent image flow between two images [28?]. Since we can sample at only 10 discrete time points during inference, we hypothesize that we only need to train the denoiser ϵ_θ at those 10 time steps, not necessarily at all the 1,000 time points.

Training and Sampling of Fast-DDPM In this paper, Fast-DDPM is applied to conditional image-to-image generation. For each image x_0 sampled from $p_{\text{data}}(x_0)$, we assume there are one or more associated condition images, denoted by c . Here, c may represent either a single image or multiple images, depending on the specific application. We denote the joint distribution of x_0 and c as $p_{\text{joint}}(x_0, c)$ and the marginal distribution of the conditional image as $p_c(c)$. We will train a conditional image denoiser $\epsilon_\theta(x(t), c, t)$ that takes the condition c as an additional input to guide the estimation of the score function at each time t . We used the following simple loss function that assigns equal weights to different times t :

$$\mathbb{E}_{i, (x_0, c), \epsilon} \|\epsilon - \epsilon_\theta(\alpha(t)x_0 + \sigma(t)\epsilon, c, t)\|^2 \quad (9)$$

where $T = 10$, $i \in \{1, 2, \dots, T\}$, $t = \frac{i}{T}$, $(x_0, c) \sim p_{\text{joint}}(x_0, c)$, and $\epsilon \sim \mathcal{N}(0, \mathbb{I})$.

The sampling process starts by randomly sampling a Gaussian noise $x(1) \sim \mathcal{N}(0, \mathbb{I})$ and a condition image $c \sim p_c(c)$. The DDIM sampler [31] was used to solve the reverse-time ODE to obtain the noise-free output x_0 that corresponds to c . We summarize the training and sampling processes of Fast-DDPM in Algorithm 1 and Algorithm 2, respectively.

Algorithm 1: Training Fast-DDPM

```

1 repeat
2    $i \in \{1, \dots, T\}$ 
3    $(x_0, c) \sim p_{\text{joint}}(x_0, c)$ 
4    $\epsilon \sim \mathcal{N}(0, \mathbb{I})$ 
5    $t = \frac{i}{T}$ 
6   Gradient descent:
      $\nabla_\theta \|\epsilon - \epsilon_\theta(\alpha(t)x_0 + \sigma(t)\epsilon, c, t)\|^2$ 
7 until converged;
```

Algorithm 2: Sampling Fast-DDPM

```

1  $x(1) \sim \mathcal{N}(0, \mathbb{I})$ 
2  $c \sim p_c(c)$ 
3 for  $i = T, \dots, 1$  do
4    $t = \frac{i}{T}$ 
5    $x(t - \frac{1}{T}) = \frac{\alpha(t - \frac{1}{T})}{\alpha(t)}x(t) + [\sigma(t - \frac{1}{T}) - \frac{\alpha(t - \frac{1}{T})}{\alpha(t)}\sigma(t)]\epsilon_\theta(x(t), c, t)$ 
6 end
7 return  $x(0)$ 
```

4 Experiments

We evaluated our Fast-DDPM model on three medical image-to-image tasks: multi-image super-resolution, image denoising, and image-to-image translation.

4.1 Datasets

Prostate MRI Dataset for Multi-Image Super-Resolution. We used T2-weighted (T2w) prostate MRI scans from the publicly available Prostate-MRI-US-Biopsy dataset [33]. The in-plane resolution of each MRI is $0.547\text{mm} \times 0.547\text{mm}$, with a 1.5mm distance between adjacent slices. An image triplet, comprising three consecutive MRI images, serves as a single training or testing example. In this setup, the first and third slices serve as inputs to the model, while the middle slice is considered as the ground truth. We used a total of 6979 image triplets from 120 MRI volumes for training and 580 image triplets from 10 MRI volumes for testing. All MRI slices were resized to 256×256 and normalized to the range $[-1, 1]$.

Low-Dose and Full-Dose Lung CT Dataset for Image Denoising. We used paired low-dose and normal-dose chest CT image volumes from the publicly available LDCT-and-Projection-data dataset [25]. The normal-dose CT scans were acquired at routine dose levels, while the low-dose CT scans were reconstructed using simulated lower dose levels, specifically at 10% of the routine dose. We randomly selected 38 patients for training and the 10 patients for evaluation, comprising 13,211 and 3,501 2D low-dose and normal-dose CT image pairs, respectively. All images were resized to 256×256 and normalized to $[-1, 1]$.

BraTS Brain MRI Dataset for Image-to-Image Translation. We used registered T1-weighted (T1w) and T2-weighted (T2w) MR images from the publicly available BraTS 2018 dataset [27]. All images were resampled to a resolution of 1 mm^3 and skull-stripped. Our focus was on converting T1w MRI into T2w MRI. The dataset, obtained from [19], comprised 5760 pairs of T1w and T2w MR images for training and 768 pairs for testing. All MRI slices were padded from 224×224 to 256×256 and normalized to $[-1, 1]$.

4.2 Evaluation Metrics

In all three image-to-image generation tasks, we used the peak signal-to-noise ratio (PSNR) and the structural similarity index measure (SSIM) to evaluate the similarity between the generated image and the ground truth image. PSNR measures the ratio between the maximum possible value (power) of the ground truth image and the power of distorting noise:

$$PSNR = 20 \cdot \log_{10} \left(\frac{MAX_I}{\sqrt{MSE}} \right) \quad (10)$$

where MAX_I denotes the maximum possible pixel value of the image and MSE denotes the mean squared error. SSIM [36] is a widely used metric that measures the structural similarity between two images and aligns better with human perception of image quality. SSIM is defined as:

$$SSIM(x, \hat{x}) = \frac{2\mu_x\mu_{\hat{x}} + c_1}{\mu^2_x + \mu^2_{\hat{x}} + c_1} \cdot \frac{2\sigma_{x\hat{x}} + c_2}{\sigma^2_x + \sigma^2_{\hat{x}} + c_2} \quad (11)$$

where $\mu_x, \mu_{\hat{x}}$ and $\sigma_x, \sigma_{\hat{x}}$ are the means and standard deviations of image x and image \hat{x} , respectively; $\sigma_{x\hat{x}}$ denotes the covariance of x and \hat{x} . The value of c_1 is $(k_1L)^2$ and $c_2 = (k_2L)^2$, where k_1 is 0.01, k_2 is 0.03, and L denotes the largest pixel value of the image x .

4.3 Training Details

Fast-DDPM adopted the hyperparameter settings and the UNet architecture from DDIM [31]. For the image super-resolution task, we used the noise scheduler with non-uniform sampling, and for the denoising and translation tasks, we used the noise scheduler with uniform sampling. We used a training batch size of 16 and trained the Fast-DDPM model for 400,000 iterations and the DDPM model for 2 million iterations. The Adam optimizer with a learning rate of 2×10^{-4} was used for training. All experiments were conducted on a computing node with 4 NVIDIA A100 GPUs, each with 80GB memory. We used Python 3.10.6 and PyTorch 1.12.1 for all experiments.

5 Results

Given that DDPM is the most widely used diffusion model in medical imaging, we focused on comparing Fast-DDPM against DDPM and current state-of-the-art methods for each task.

5.1 Multi-Image Super-Resolution

Results in Table 1 show that Fast-DDPM outperformed DDPM, miSRCNN [6] (based on convolutional neural networks), and miSRGAN [34] (based on generative adversarial networks). Notably, Fast-DDPM significantly improved DDPM’s performance, increasing PSNR from 25.3 to 27.1 and SSIM from 0.83 to 0.89. Fast-DDPM also significantly improved computational efficiency compared to DDPM, reducing training time from 136 hours to 26 hours and per volume inference time from 3.7 minutes to 2.3 seconds.

Table 1: Comparison of the performance and inference time per image volume (an average of 58 slices) for various multi-image super-resolution methods.

Method	PSNR	SSIM	Training time	Inference Time
miSRCNN [6]	26.5	0.87	1 h	0.01s
miSRGAN [34]	26.8	0.88	40 h	0.04 s
DDPM [9]	25.3	0.83	136 h	3.7 m
Fast-DDPM	27.1	0.89	26 h	2.3 s

Figure 4 shows the results of various image super-resolution methods on a representative subject. The models received the previous and next slices as inputs, with the center slice serving as the ground truth. It is evident that the miSRCNN and miSRGAN methods failed to accurately reconstruct the shadowed area highlighted by the arrows. In contrast, Fast-DDPM most effectively reconstructed the information missing between the previous and next 2D slices. Interestingly, although DDPM is qualitatively inferior to miSRCNN and miSRGAN, it visually outperformed both methods.

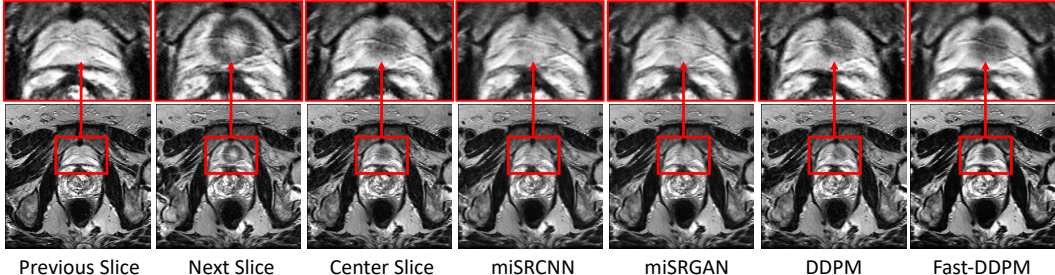


Figure 4: Qualitative results of the MR multi-image super-resolution task.

5.2 Image Denoising

The results presented in Table 2 indicate that Fast-DDPM significantly outperformed the DDPM model, as well as two other prominent CT denoising methods, REDCNN [2] and DU-GAN [12]. In terms of computational efficiency, Fast-DDPM reduced the inference time by approximately 100-fold and the training time by 5-fold compared to DDPM. Notably, the performance of the original DDPM model was inferior to that of REDCNN and DU-GAN. By implementing an efficient training strategy, Fast-DDPM significantly improve the PSNR and SSIM, achieving state-of-the-art performance.

Table 2: Comparison of the performance and inference time per image volume (an average of 360 slices) for various CT image denoising methods.

Method	PSNR	SSIM	Training time	Inference Time
REDCNN [2]	36.4	0.91	3 h	0.5 s
DU-GAN [12]	36.3	0.90	20 h	3.8 s
DDPM [9]	35.4	0.87	141 h	21.4 m
Fast-DDPM	37.5	0.92	26 h	12.5 s

Figure 5 shows the low-dose, normal-dose, and predicted normal-dose CT images by various models of a representative subject. The zoomed-in region, highlighted by the red rectangular boxes, demonstrate the capability of our Fast-DDPM model to preserve detailed structures in the denoised images

compared to other methods. Notably, the lung fissure appears clear and sharp in the image generated by Fast-DDPM, while the other methods exhibit noticeable blurring and loss of details in this region. A pulmonary fissure is a boundary between the lobes in the lungs. The preserved details of the fissure allow for automated segmentation of the lung fissure, facilitating further analysis of lung disease at a lobar level.

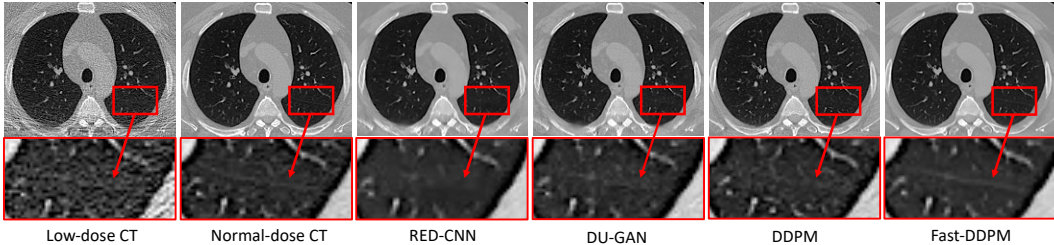


Figure 5: Qualitative results of the CT image denoising task.

5.3 Image-to-Image Translation

Results in Table 3 show that Fast-DDPM and DDPM outperformed leading methods in the image-to-image translation task, including Pix2Pix [14] and RegGAN [19]. Although DDPM achieved performance comparable to Fast-DDPM, Fast-DDPM significantly reduced the training time from 135 hours to 27 hours and the sampling time from 22.2 minutes per batch to 13.2 seconds per batch. This highlights the practical advantages of Fast-DDPM in real-world applications. Moreover, extending the training period for Fast-DDPM (denoted as Fast-DDPM*) enhanced its SSIM score from 0.89 to 0.91.

Table 3: Comparison of the performance and averaged inference time per batch (360 slices) for various image-to-image translation methods.

Method	PSNR	SSIM	Training time	Inference Time
Pix2Pix [14]	25.6	0.85	6 h	3.3 s
RegGAN [19]	26.0	0.86	9 h	3.1 s
DDPM [9]	26.3	0.89	135 h	22.2 m
Fast-DDPM	26.3	0.89	27 h	13.2 s
Fast-DDPM*	26.3	0.91	133 h	13.2 s

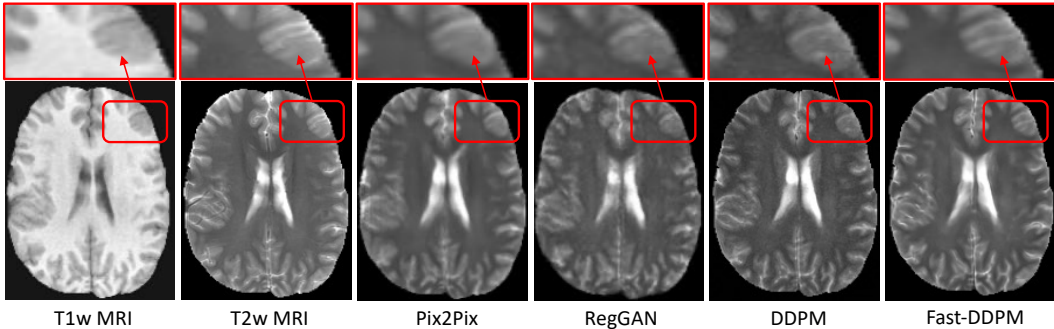


Figure 6: Qualitative results of the T1w MRI to T2w MRI translation task.

Figure 6 shows the T2w MR images generated by various image-to-image translation methods for a representative subject. Notably, predictions by the Pix2Pix and RegGAN models are blurry and fail to reconstruct the intricate structures in the brain region highlighted by the arrows. Although the DDPM model recovered some of the details in the MRI, its reconstructed T2 MRI has a relatively lower signal-to-noise ratio. The Fast-DDPM model demonstrates its ability to generate high-quality translated images with better structural details and less noise.

5.4 Ablation Study

Impact of the Number of Time Steps. We investigated the impact of the number of time steps on the performance of Fast-DDPM. Specifically, we conducted experiments using 5, 10, 20, 50, 100, and 1000 time steps across all three datasets. The results in Table 4 indicate that the number of time steps significantly affects the performance of Fast-DDPM in different image-to-image tasks. Optimal performance for image super-resolution and image denoising is achieved with 10 time steps. For the image-to-image translation task, where the condition (c) and the output (x_0) have significantly different intensity levels, the best performance is achieved using 100 time steps. For all tasks, performance declines with more than 100 time steps. These findings underscore the importance of carefully tuning the number of time steps for specific tasks to balance computational efficiency and image quality. Future work could explore adaptive mechanisms for dynamically adjusting time steps based on input complexity and task requirements.

Table 4: The impact of the number of time steps on different image-to-image tasks.

Number of Time Steps	Super-Resolution		Denoising		Translation	
	PSNR	SSIM	PSNR	SSIM	PSNR	SSIM
5	26.9	0.88	37.4	0.92	25.8	0.91
10	27.1	0.89	37.5	0.92	26.3	0.91
20	26.7	0.88	37.4	0.91	26.5	0.91
50	26.2	0.87	36.9	0.91	26.5	0.92
100	25.8	0.86	36.5	0.90	26.6	0.92
1000	25.3	0.83	35.4	0.87	26.3	0.89

Impact of Noise Scheduler. Table 5 illustrates the impact of the two proposed noise schedulers on the performance of Fast-DDPM. The uniform noise scheduler is a better choice for image denoising and image-to-image translation tasks, while the non-uniform noise scheduler performed better in the super-resolution task. These findings highlight the importance of selecting an appropriate noise scheduler tailored to the specific image-to-image task. This adaptability enhances Fast-DDPM’s performance across various medical image processing applications, demonstrating its versatility and effectiveness in handling diverse imaging challenges.

Table 5: The impact of two proposed noise schedulers on different image-to-image tasks.

Noise Scheduler	Super-Resolution		Denoising		Translation	
	PSNR	SSIM	PSNR	SSIM	PSNR	SSIM
Uniform	26.6	0.88	37.5	0.92	26.3	0.91
Non-uniform	27.1	0.89	37.3	0.91	26.1	0.90

6 Discussion and Conclusion

This paper introduces Fast-DDPM, a simple yet effective approach that accelerates both the training and sampling of DDPM while significantly improving its performance. Our evaluation demonstrates that Fast-DDPM achieves state-of-the-art performance across various medical image-to-image generation tasks.

Limitations and Future Work The noise schedulers used in this study were manually designed and optimized for the specific tasks, this approach may not be optimal for all types of medical imaging tasks. Future work should focus on developing adaptive noise schedulers that can dynamically adjust based on the complexity of the input data and the specific requirements of the imaging task.

Broader Impact The advancements introduced by Fast-DDPM have significant implications for the field of medical imaging. The dramatic reduction in computational resources required for training and sampling makes diffusion models more accessible and practical for real-world clinical applications. This can lead to faster and more accurate diagnosis and treatment planning, ultimately improving patient outcomes.

References

- [1] Chentao Cao, Zhuo-Xu Cui, Yue Wang, Shaonan Liu, Taijin Chen, Hairong Zheng, Dong Liang, and Yanjie Zhu. High-frequency space diffusion model for accelerated mri. *IEEE Transactions on Medical Imaging*, pages 1–1, 2024.
- [2] Hu Chen, Yi Zhang, Mannudeep K Kalra, Feng Lin, Yang Chen, Peixi Liao, Jiliu Zhou, and Ge Wang. Low-dose ct with a residual encoder-decoder convolutional neural network. *IEEE transactions on medical imaging*, 36(12):2524–2535, 2017.
- [3] Ting Chen. On the importance of noise scheduling for diffusion models. *arXiv preprint arXiv:2301.10972*, 2023.
- [4] Hyungjin Chung, Eun Sun Lee, and Jong Chul Ye. Mr image denoising and super-resolution using regularized reverse diffusion. *IEEE Transactions on Medical Imaging*, 42(4):922–934, 2023.
- [5] Prafulla Dhariwal and Alexander Nichol. Diffusion models beat gans on image synthesis. *Advances in neural information processing systems*, 34:8780–8794, 2021.
- [6] Chao Dong, Chen Change Loy, Kaiming He, and Xiaoou Tang. Image super-resolution using deep convolutional networks. *IEEE transactions on pattern analysis and machine intelligence*, 38(2):295–307, 2015.
- [7] Kuang Gong, Keith Johnson, Georges El Fakhri, Quanzheng Li, and Tinsu Pan. Pet image denoising based on denoising diffusion probabilistic model. *European Journal of Nuclear Medicine and Molecular Imaging*, pages 1–11, 2023.
- [8] Alper Güngör, Salman UH Dar, Şaban Öztürk, Yılmaz Korkmaz, Hasan A. Bedel, Gokberk Elmas, Muzaffer Ozbey, and Tolga Çukur. Adaptive diffusion priors for accelerated mri reconstruction. *Medical Image Analysis*, 88:102872, 2023.
- [9] Jonathan Ho, Ajay Jain, and Pieter Abbeel. Denoising diffusion probabilistic models. *Advances in neural information processing systems*, 33:6840–6851, 2020.
- [10] Emiel Hoogeboom, Jonathan Heek, and Tim Salimans. simple diffusion: End-to-end diffusion for high resolution images. In *International Conference on Machine Learning*, pages 13213–13232. PMLR, 2023.
- [11] Xinrong Hu, Yu-Jen Chen, Tsung-Yi Ho, and Yiyu Shi. Conditional diffusion models for weakly supervised medical image segmentation, 2023.
- [12] Zhizhong Huang, Junping Zhang, Yi Zhang, and Hongming Shan. Du-gan: Generative adversarial networks with dual-domain u-net-based discriminators for low-dose ct denoising. *IEEE Transactions on Instrumentation and Measurement*, 71:1–12, 2021.
- [13] Hasan Iqbal, Umar Khalid, Chen Chen, and Jing Hua. Unsupervised anomaly detection in medical images using masked diffusion model. In Xiaohuan Cao, Xuanang Xu, Islem Rekik, Zhiming Cui, and Xi Ouyang, editors, *Machine Learning in Medical Imaging*, pages 372–381, Cham, 2024. Springer Nature Switzerland.
- [14] Phillip Isola, Jun-Yan Zhu, Tinghui Zhou, and Alexei A Efros. Image-to-image translation with conditional adversarial networks. In *Proceedings of the IEEE conference on computer vision and pattern recognition*, pages 1125–1134, 2017.
- [15] Boah Kim, Inhwa Han, and Jong Chul Ye. Diffusemorph: Unsupervised deformable image registration using diffusion model. In Shai Avidan, Gabriel Brostow, Moustapha Cissé, Giovanni Maria Farinella, and Tal Hassner, editors, *Computer Vision – ECCV 2022*, pages 347–364, Cham, 2022. Springer Nature Switzerland.
- [16] Boah Kim, Yujin Oh, and Jong Chul Ye. Diffusion adversarial representation learning for self-supervised vessel segmentation. In *The Eleventh International Conference on Learning Representations*, 2023.

- [17] Jonghun Kim and Hyunjin Park. Adaptive latent diffusion model for 3d medical image to image translation: Multi-modal magnetic resonance imaging study. In *Proceedings of the IEEE/CVF Winter Conference on Applications of Computer Vision (WACV)*, pages 7604–7613, January 2024.
- [18] Diederik Kingma, Tim Salimans, Ben Poole, and Jonathan Ho. Variational diffusion models. *Advances in neural information processing systems*, 34:21696–21707, 2021.
- [19] Lingke Kong, Chenyu Lian, Detian Huang, ZhenJiang Li, Yanle Hu, and Qichao Zhou. Breaking the dilemma of medical image-to-image translation. In *Thirty-Fifth Conference on Neural Information Processing Systems*, 2021.
- [20] Vladimir Kulikov, Shahar Yadin, Matan Kleiner, and Tomer Michaeli. Sinddm: A single image denoising diffusion model. In *International Conference on Machine Learning*, pages 17920–17930. PMLR, 2023.
- [21] Jiaming Liu, Rushil Anirudh, Jayaraman J. Thiagarajan, Stewart He, K Aditya Mohan, Ulugbek S. Kamilov, and Hyojin Kim. Dolce: A model-based probabilistic diffusion framework for limited-angle ct reconstruction. In *Proceedings of the IEEE/CVF International Conference on Computer Vision (ICCV)*, pages 10498–10508, October 2023.
- [22] Cheng Lu, Yuhao Zhou, Fan Bao, Jianfei Chen, Chongxuan Li, and Jun Zhu. Dpm-solver: A fast ode solver for diffusion probabilistic model sampling in around 10 steps. *Advances in Neural Information Processing Systems*, 35:5775–5787, 2022.
- [23] Qing Lyu and Ge Wang. Conversion between ct and mri images using diffusion and score-matching models, 2022.
- [24] Jun Ma, Yuanzhi Zhu, Chenyu You, and Bo Wang. Pre-trained diffusion models for plug-and-play medical image enhancement. In Hayit Greenspan, Anant Madabhushi, Parvin Mousavi, Septimiu Salcudean, James Duncan, Tanveer Syeda-Mahmood, and Russell Taylor, editors, *Medical Image Computing and Computer Assisted Intervention – MICCAI 2023*, pages 3–13, Cham, 2023. Springer Nature Switzerland.
- [25] C McCollough, B Chen, D Holmes, X Duan, Z Yu, L Xu, S Leng, and J Fletcher. Low dose ct image and projection data (ldct-and-projection-data)(version 4). *Med. Phys.*, 48:902–911, 2021.
- [26] Chenlin Meng, Robin Rombach, Ruiqi Gao, Diederik Kingma, Stefano Ermon, Jonathan Ho, and Tim Salimans. On distillation of guided diffusion models. In *Proceedings of the IEEE/CVF Conference on Computer Vision and Pattern Recognition*, pages 14297–14306, 2023.
- [27] Bjoern H Menze, Andras Jakab, Stefan Bauer, Jayashree Kalpathy-Cramer, Keyvan Farahani, Justin Kirby, Yuliya Burren, Nicole Porz, Johannes Slotboom, Roland Wiest, et al. The multimodal brain tumor image segmentation benchmark (brats). *IEEE transactions on medical imaging*, 34(10):1993–2024, 2014.
- [28] Michael I Miller, Alain Trouvé, and Laurent Younes. Geodesic shooting for computational anatomy. *Journal of mathematical imaging and vision*, 24:209–228, 2006.
- [29] Muzaffer Özbey, Onat Dalmaz, Salman UH Dar, Hasan A Bedel, Şaban Öztürk, Alper Güngör, and Tolga Çukur. Unsupervised medical image translation with adversarial diffusion models. *IEEE Transactions on Medical Imaging*, 2023.
- [30] Tim Salimans and Jonathan Ho. Progressive distillation for fast sampling of diffusion models. *arXiv preprint arXiv:2202.00512*, 2022.
- [31] Jiaming Song, Chenlin Meng, and Stefano Ermon. Denoising diffusion implicit models. *arXiv preprint arXiv:2010.02502*, 2020.
- [32] Yang Song, Jascha Sohl-Dickstein, Diederik P Kingma, Abhishek Kumar, Stefano Ermon, and Ben Poole. Score-based generative modeling through stochastic differential equations. *arXiv preprint arXiv:2011.13456*, 2020.

- [33] Geoffrey A Sonn, Shyam Natarajan, Daniel JA Margolis, Malu MacAiran, Patricia Lieu, Jiaoti Huang, Frederick J Dorey, and Leonard S Marks. Targeted biopsy in the detection of prostate cancer using an office based magnetic resonance ultrasound fusion device. *The Journal of urology*, 189(1):86–92, 2013.
- [34] Rewa R Sood, Wei Shao, Christian Kunder, Nikola C Teslovich, Jeffrey B Wang, Simon JC Soerensen, Nikhil Madhuripan, Anugayathri Jawahar, James D Brooks, Pejman Ghanouni, et al. 3d registration of pre-surgical prostate mri and histopathology images via super-resolution volume reconstruction. *Medical image analysis*, 69:101957, 2021.
- [35] Jueqi Wang, Jacob Levman, Walter Hugo Lopez Pinaya, Petru-Daniel Tudosiu, M. Jorge Cardoso, and Razvan Marinescu. Inverser: 3d brain mri super-resolution using a latent diffusion model. In Hayit Greenspan, Anant Madabhushi, Parvin Mousavi, Septimiu Salcudean, James Duncan, Tanveer Syeda-Mahmood, and Russell Taylor, editors, *Medical Image Computing and Computer Assisted Intervention – MICCAI 2023*, pages 438–447, Cham, 2023. Springer Nature Switzerland.
- [36] Zhou Wang, A.C. Bovik, H.R. Sheikh, and E.P. Simoncelli. Image quality assessment: from error visibility to structural similarity. *IEEE Transactions on Image Processing*, 13(4):600–612, 2004.
- [37] Julia Wolleb, Florentin Bieder, Robin Sandkühler, and Philippe C. Cattin. Diffusion models for medical anomaly detection. In Linwei Wang, Qi Dou, P. Thomas Fletcher, Stefanie Speidel, and Shuo Li, editors, *Medical Image Computing and Computer Assisted Intervention – MICCAI 2022*, pages 35–45, Cham, 2022. Springer Nature Switzerland.
- [38] Zhanxiong Wu, Xuanheng Chen, Sangma Xie, Jian Shen, and Yu Zeng. Super-resolution of brain mri images based on denoising diffusion probabilistic model. *Biomedical Signal Processing and Control*, 85:104901, 2023.
- [39] Zhaohu Xing, Liang Wan, Huazhu Fu, Guang Yang, and Lei Zhu. Diff-unet: A diffusion embedded network for volumetric segmentation, 2023.
- [40] Rui Xu, Yunke Wang, and Bo Du. Maediff: Masked autoencoder-enhanced diffusion models for unsupervised anomaly detection in brain images, 2024.
- [41] Hongkai Zheng, Weili Nie, Arash Vahdat, Kamyar Azizzadenesheli, and Anima Anandkumar. Fast sampling of diffusion models via operator learning. In *International Conference on Machine Learning*, pages 42390–42402. PMLR, 2023.